Journal of Medicinal Chemistry

pubs.acs.org/jmc

Article

Synthesis and Evaluation of ^{99m}Tc-Labeled L-Aspartic Acid as a EuK Polymer Linker for Targeting PSMA to a Novel SPECT Tumor Tracer

Zuojie Li, Xiaojiang Duan, Peiwen Han, Guangxing Yin, Yuhao Jiang, Qing Ruan, and Junbo Zhang*

Cite This: *J. Med. Chem.* 2024, 67, 21617−21628

Read Online

ACCESS | Metrics & More | Article Recommendations | Supporting Information

ABSTRACT: The development of novel tracers targeting prostate-specific membrane antigen (PSMA) has great potential for improving the diagnosis and treatment of prostate cancer (PCa). This study aimed to improve the absolute tumor uptake and tumor-to-background ratios (TBRs) of this novel PSMA tracer by increasing the number of pharmacophores, Glu-urea-Lys (EuK), that specifically bind to PSMA. We successfully synthesized four radioligands and prepared a total of 12 stable radiotracers by coordinating ^{99m}Tc with various coligands. [^{99m}Tc]Tc-EUKD-EDDA showed the best pharmacokinetic properties both *in vitro* and *in vivo*. It effectively increased the absolute uptake in tumors and resulted in good tumor retention. Rapid clearance in nontarget organs resulted in high TBRs. High-contrast SPECT/CT images were obtained within 2−6 h after injection, suggesting that [^{99m}Tc]Tc-EUKD-EDDA has great application potential in time-lapse imaging of PCa, which is important for improving the diagnostic accuracy of PCa in clinical practice.

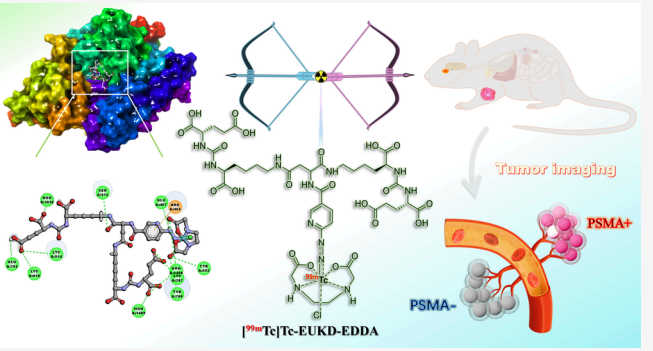

INTRODUCTION

Prostate cancer (PCa) is the most common malignant tumor of the male reproductive system.[1−3] The incidence and mortality of PCa are increasing worldwide from year to year.[4−6] PCa is considered the second leading cause of death in males after heart disease and is an important global public health issue.[7,8] The early symptoms of PCa are not obvious, and most patients are already in the late stage at diagnosis, missing the best time for treatment.[9,10] Therefore, the effective diagnosis of PCa is highly important for the treatment and prognosis of patients.

The technique known as "radiotracer diagnosis" uses a tracer that has been labeled with a radioactive isotope to identify PCa. Radiotracers are valuable tools for clinical PCa diagnosis because they have unique advantages over other diagnostic techniques, such as prostate-specific antigen (PSA) testing, rectal examination, prostate ultrasound, and prostate puncture biopsy.[11] These advantages include high specificity, high sensitivity, and noninvasiveness, which reduces the patient's risk and pain.[12−16] Currently, four radiotracers targeting prostate-specific membrane antigen (PSMA) have been approved for clinical PCa diagnosis or treatment, which can be divided into two main categories: positron emission tomography (PET) and single-photon emission computed tomography (SPECT). [^{68}Ga]Ga-PSMA11, [^{18}F]F-DCFPyL, [^{18}F]F-rhPSMA-7.3 and [^{177}Lu]Lu-PSMA-617 provide high accuracy for detecting or treating PSMA-positive lesions in male cancer patients, but their sensitivity is strongly affected by the PSA concentration in the body and they often accumulate in nontarget organs such as the kidneys, bladder and salivary glands, which may cause diagnostic interference and limit the effective diagnosis of early PCa with low PSA expression.[17−21]

In recent years, increasing the number of target groups has become a viable strategy for improving the performance of radiotracers.[22,23] Based on studies of dimers and polymers, radiotracers have shown obvious advantages in increasing absolute tumor uptake, reducing uptake in nontarget organs, and improving tumor-to-background ratios (TBRs). For example, the radiotracers [^{68}Ga]7 ([EuK]$_2$-HBED-CC), [^{68}Ga]Ga-PSMA-D5 ([EuK]$_2$-DOTA) and [^{68}Ga]Ga-DOTA-(2P-PEG$_4$)$_2$ ([EuK]$_4$-DOTA), developed by increasing the number of Glu-urea-Lys (EuK) oligopeptides (PSMA targeting groups), effectively increased tumor uptake by almost 2-fold compared with that of their monomers, and their TBRs clearly improved.[24−26] Moreover, the same benefits have been demonstrated in the development of radiotracers for targets such as fibroblast activation protein (FAP) and integrins,[27−29] such as [^{68}Ga]Ga-DOTA-2P(FAPI)$_2$, [^{68}Ga]Ga-DOTA-4P-(FAPI)$_4$ and [^{99m}Tc]Tc-3PRGD$_2$, etc. These results highlight the significant impact of the modification strategy of increasing

Received: October 31, 2024
Revised: November 24, 2024
Accepted: November 27, 2024
Published: December 3, 2024

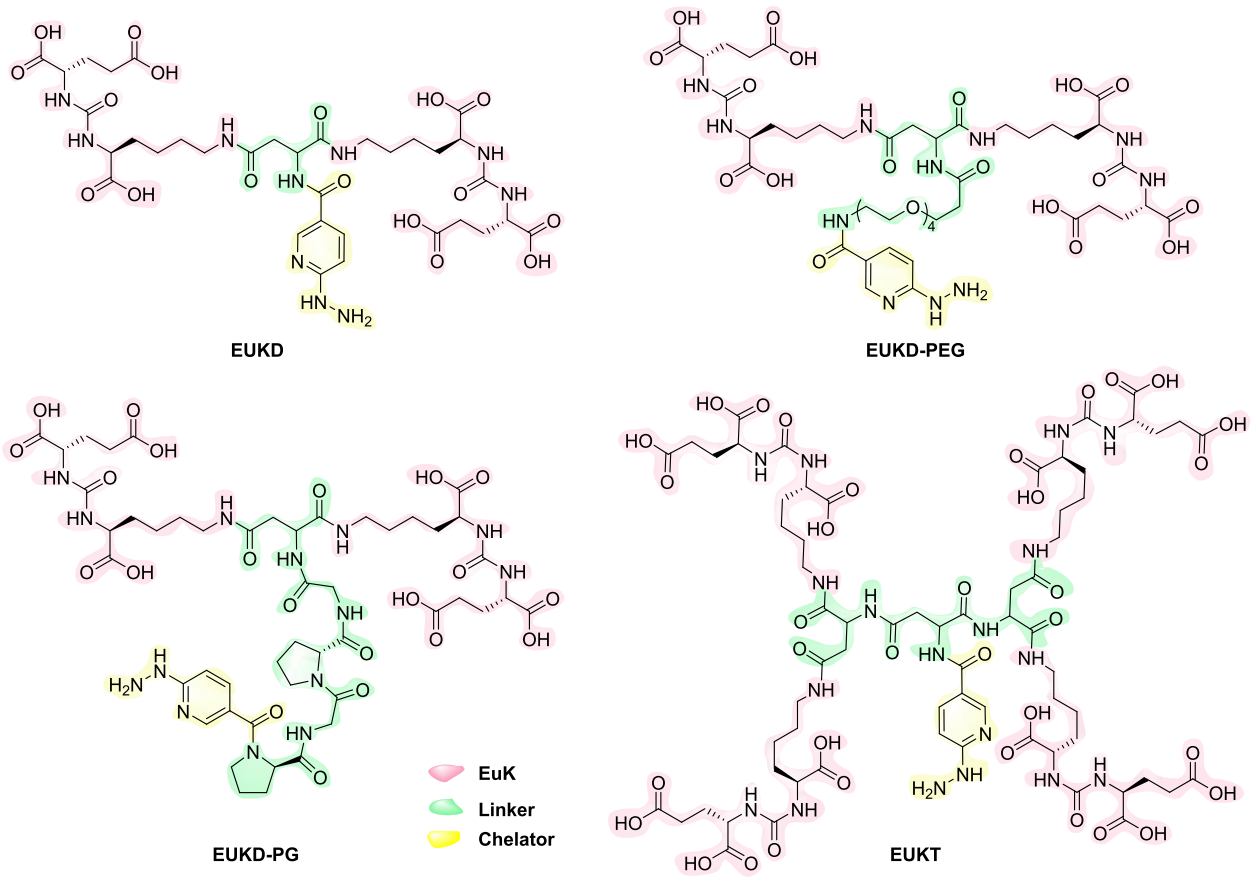

Figure 1. Structures of PSMA dimeric and tetrameric radioligands.

the number of target groups on the improvement of radioligands. Therefore, adjusting the number of EuK groups (EuKs) to improve the performance of PSMA radiotracers is reasonable and feasible.

For radiotracers, linkers between targeting groups and between targeting groups and radionuclide chelators play an important role in improving pharmacokinetic (PK) properties. $_D$Pro-Gly (PG) oligopeptide chains and polyethylene glycol (PEG) chains are widely used to regulate PK properties.[30] In previous studies, our research group examined the effects of the linker types between the targeting group and the radionuclide chelators on the performance of FAP radiotracers.[31−33] Studies have shown that PG and PEG chains have great benefits in reducing uptake into nontarget organs. Moreover, L-aspartic acid, an endogenous amino acid, has good biocompatibility and plays an important role in energy metabolism and the regulation of the acid−base balance.[34] More importantly, the amphoteric structure of the dicarboxylic acid and amino groups facilitates dimerization of the targeting group and the association of the metal chelators. For ^{99m}Tc labeling, the bifunctional chelator hydrazinonicotinamide (HYNIC) can form a stable complex with the participation of coligands.[35,36] A rich coligand composition is one of the important ways to regulate tracer stability, lipid−water distribution and targeted binding ability.

In this study, we aimed to improve the absolute tumor uptake and TBRs of novel PSMA tracers by increasing the number of EuKs. To achieve this goal, we chose L-aspartic acid as a scaffold for the polymerization of EuK-targeting groups, which were linked via stable amide bonds to form EuK dimers and tetramers and then linked to HYNIC chelators.

To further optimize our tracers, the effects of different linkers on PK properties were examined by adjusting the type of linker between HYNIC and L-aspartic acid. Radiolabeling was then carried out with ^{99m}Tc in combination with various coligands, including triphenylphosphine trisulfonate (TPPTS), diphenylphosphine benzene-3-sulfonate (TPPMS), ethylenediaminetetraacetic acid (EDDA), and N-[tris(hydroxymethyl)-methyl]glycine (tricine). We prepared two new classes of PSMA-targeting radioligands (Figure 1): dimers (EUKD, EUKD-PEG, and EUKD-PG) and tetramers (EUKT). Their PK properties and potential as SPECT imaging agents were evaluated *in vitro* and *in vivo*.

RESULTS

Chemistry. The synthesis of the PSMA dimer and tetramer radioligands is shown in Scheme 1, and initial Compounds **1** and **6** were synthesized according to our published procedure.[37] First, the dimerization of EuKs occurs via L-aspartic acid (**3**), followed by the removal of amino protecting groups via palladium−carbon reduction (**4**). In the presence of the condensing agent hexafluorophosphate azabenzotriazole tetramethyl uronium (HATU), derivatives **7** and **8** of the HYNIC groups were subsequently obtained via stable amide bonds. Finally, the targeting group was condensed with the chelating group to deprotect the protecting groups and obtain EUKD (**10a**), EUKD-PEG (**10b**), and EUKD-PEG dimers (**10c**) in 16−19% yield. The synthesis of the EUKT tetramer (**11**) was carried out by forming the EuKs tetramer (**5**) via an

https://doi.org/10.1021/acs.jmedchem.4c02656
J. Med. Chem. 2024, 67, 21617−21628

Scheme 1. Synthetic Route of PSMA Radioligands

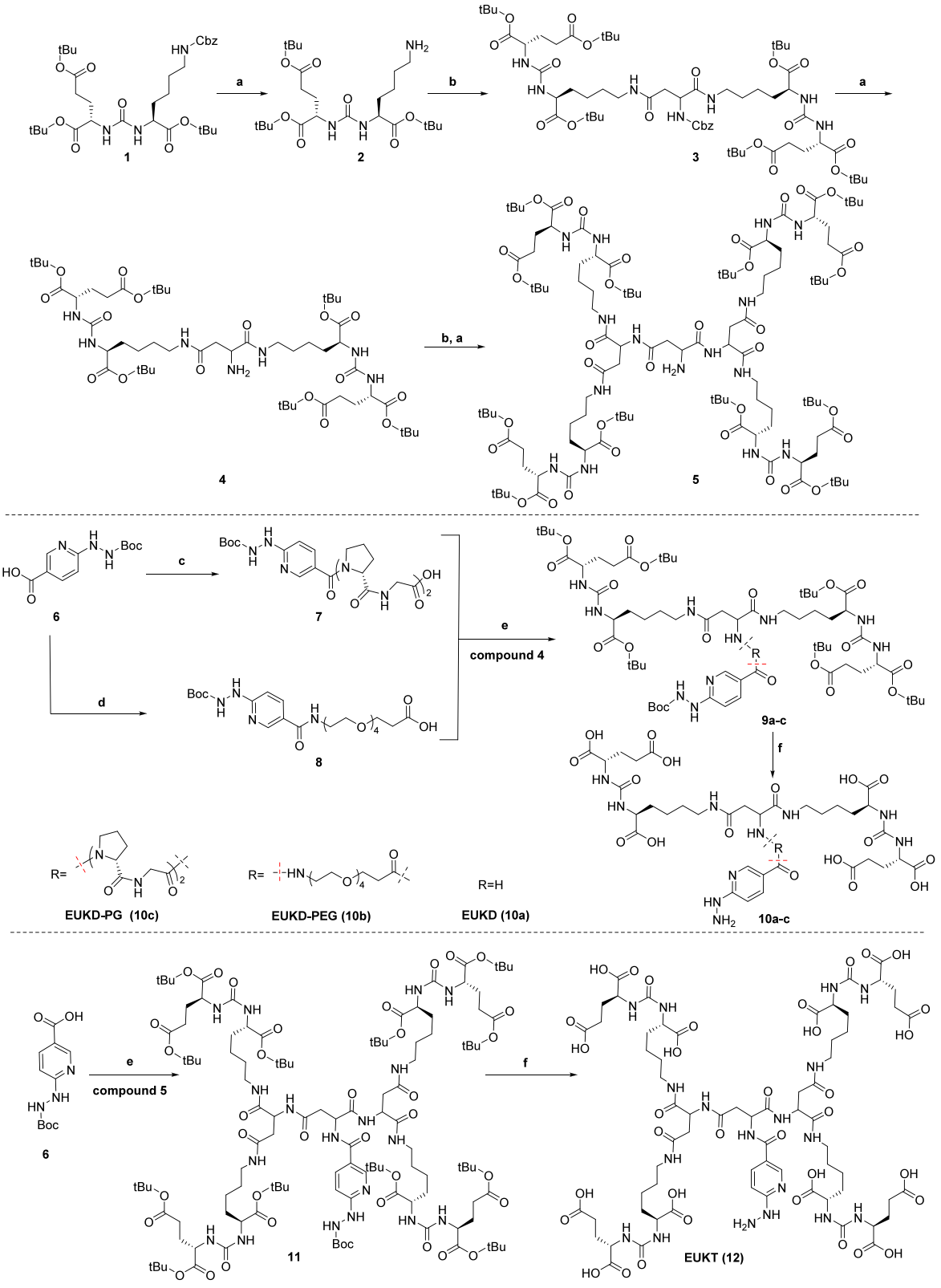

L-aspartic acid linker, followed by condensation and deprotection with a chelator (**6**) in the presence of HATU, with a yield of 26%.

Radiolabeling. As shown in Figure 2, each radioligand forms 3 stable ^{99m}Tc labels with three different coligands (TPPTS, TPPMS, and EDDA). All of the radiotracer labeling processes followed standardized protocols, and the entire labeling and analysis process was completed within 60 min. The radiochemical purities (RCP) of all of the radiotracers were greater than 90% (Figure 3**a**-**d**), and they can be used directly in subsequent studies without further purification. Among them, the retention times of [^{99m}Tc]Tc-EUKD-EDDA,

https://doi.org/10.1021/acs.jmedchem.4c02656
J. Med. Chem. 2024, 67, 21617−21628

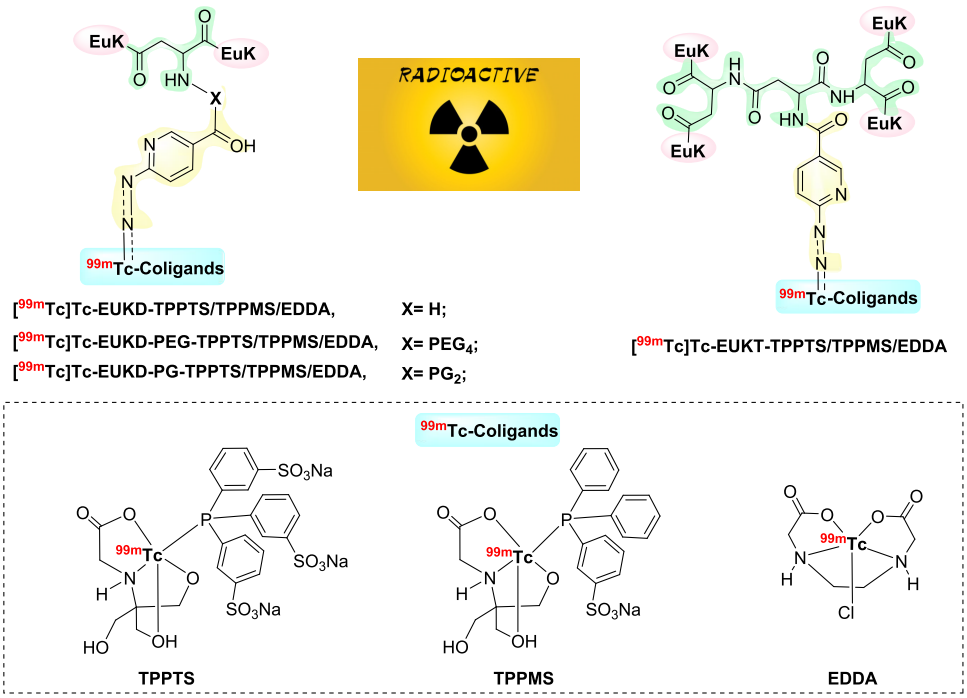

Figure 2. Speculative structure of PSMA radiotracers.

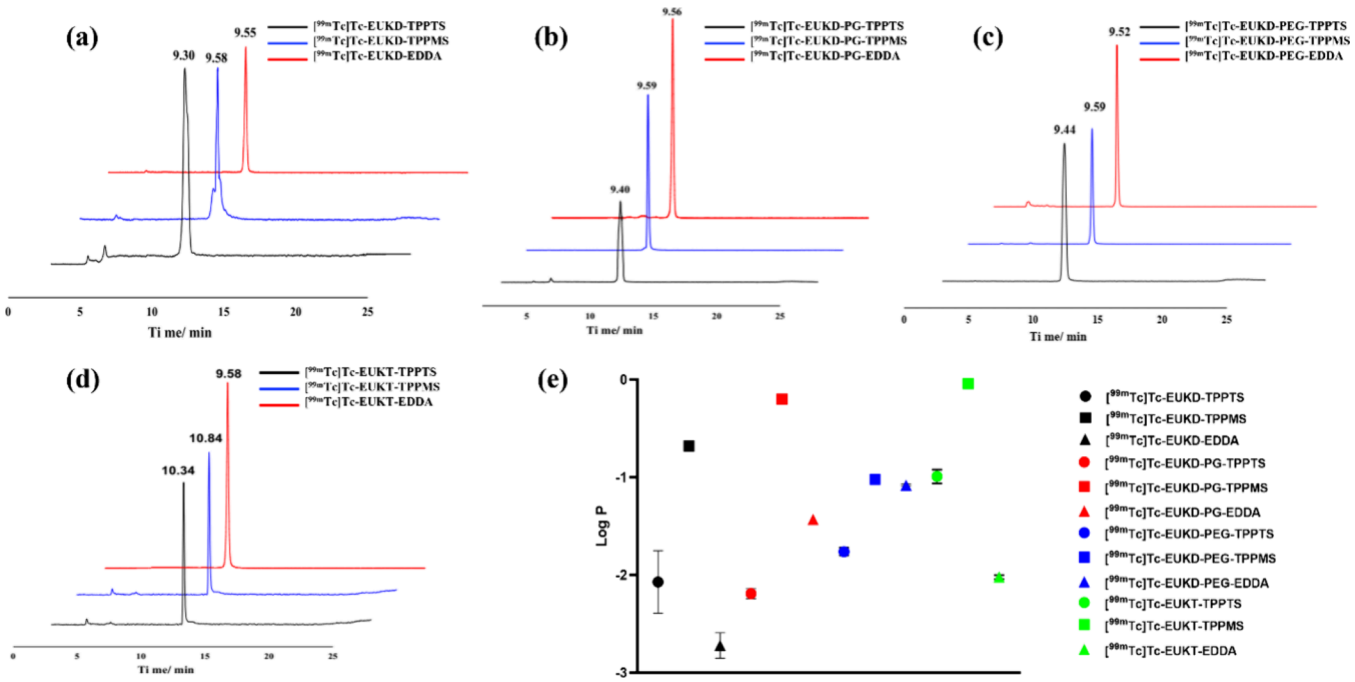

Figure 3. HPLC characterization and Log *P* of all PSMA radiotracers. (a) [^{99m}Tc]Tc-EUKD-TPPTS/TPPMS/EDDA; (b) [^{99m}Tc]Tc-EUKD-PG-TPPTS/TPPMS/EDDA; (c) [^{99m}Tc]Tc-EUKD-PEG-TPPTS/TPPMS/EDDA; (d) [^{99m}Tc]Tc-EUKT-TPPTS/TPPMS/EDDA; (e) Log *P* of PSMA radiotracers.

[^{99m}Tc]Tc-EUKD-PG-EDDA, [^{99m}Tc]Tc-EUKD-PEG-EDDA and [^{99m}Tc]Tc-EUKT-EDDA were 9.55, 9.56, 9.52, and 9.58 min, respectively. The molar activities of [^{99m}Tc]Tc-EUKD-EDDA, [^{99m}Tc]Tc-EUKD-PG-EDDA, [^{99m}Tc]Tc-EUKD-PEG-EDDA and [^{99m}Tc]Tc-EUKT-EDDA were 1.61×10^{15} Bq/mol, 2.06×10^{16} Bq/mol, 2.17×10^{16} Bq/mol and 3.15×10^{16} Bq/mol, respectively.

Stability and Log *P* Assessment. *In vitro* stability experiments (Figure S1) revealed that all of the radiotracers maintained significant stability in saline for up to 4 h, whereas four EDDA acted as coligand radiotracers ([^{99m}Tc]Tc-EUKD-EDDA, [^{99m}Tc]Tc-EUKD-PG-EDDA, [^{99m}Tc]Tc-EUKD-PEG-EDDA, [^{99m}Tc]Tc-EUKT-EDDA) and had good stability for 4 h in fresh mouse whole blood. As shown in Figure 3e and Table S1, all of the radiotracers are hydrophilic (Log *P* = −0.04 to −2.72), and [^{99m}Tc]Tc-EUKD-EDDA has the strongest hydrophilic property.

https://doi.org/10.1021/acs.jmedchem.4c02656
J. Med. Chem. 2024, 67, 21617−21628

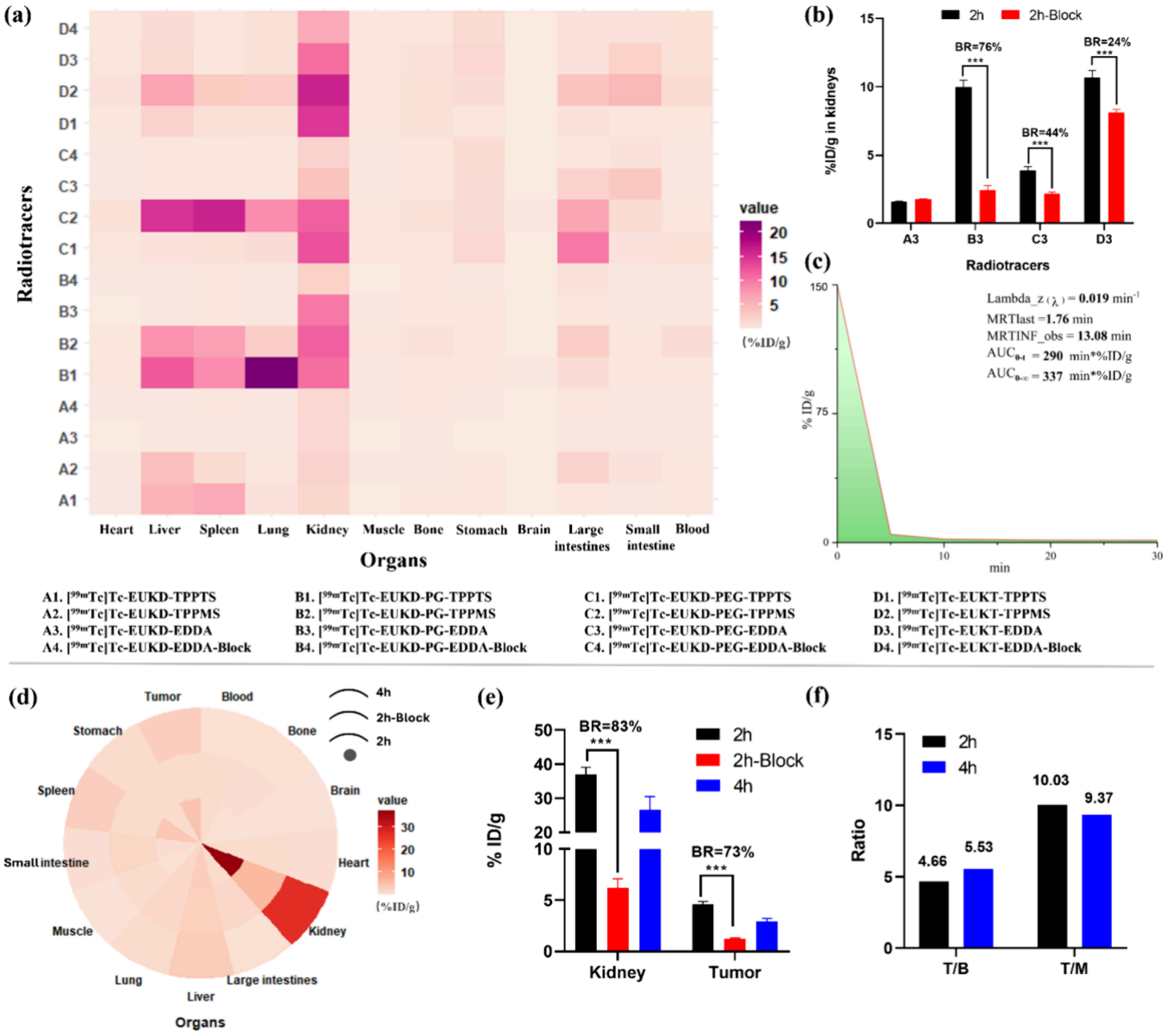

Figure 4. Biodistribution of radiotracers in mice. (a) Biodistribution in normal Kunming mice (n = 5) at 2 h after injection; (b) BR of radiotracers in the kidney; (c) blood distribution of [^{99m}Tc]Tc-EUKD-EDDA in normal Kunming mice for 5−30 min; (d) [^{99m}Tc]Tc-EUKD-EDDA biodistribution of 22Rv1 tumor-bearing mice (n = 3) at 2 h, 2 h-block and 4 h after injection; (e) BR of [^{99m}Tc]Tc-EUKD-EDDA in the kidney and tumor; (f) ratio of tumor-to-nontarget tissue in 22Rv1 tumor-bearing mice. *P < 0.05, **P < 0.01, ***P < 0.001.

Biodistribution Studies. A preliminary PK study of all of the radiotracers is shown in Figure 4a and Tables S2−S5. The uptake of all tracers in the blood, muscle and bone was less than 1% ID/g at 2 h after injection, with the highest uptake occurring in the kidney, followed by the liver and spleen. The high uptake of [^{99m}Tc]Tc-EUKD-PG-TPPTS in the lungs (22.32 ± 0.63% ID/g) and liver (12.11 ± 0.40% ID/g) may be possibly related to the formation of colloids in solution or *in vivo* environment. [^{99m}Tc]Tc-EUKT-TPPMS showed the highest uptake in the kidney (16.22 ± 0.95% ID/g), and [^{99m}Tc]Tc-EUKD-EDDA showed the lowest uptake (1.58 ± 0.06% ID/g). Compared with the TPPTS and TPPMS coligands, among the four radioligands, EDDA effectively reduced kidney uptake by almost 1 to 3 times, liver uptake by almost 5 to 100-fold, and spleen uptake by almost 1 to 50-fold. The renal blocking rate (BR) of the preinjected PSMA blockers 2-PMPA, [^{99m}Tc]Tc-EUKD-PG-EDDA, [^{99m}Tc]Tc-EUKD-PEG-EDDA and [^{99m}Tc]Tc-EUKT-EDDA were 76% (10.00 ± 0.50 vs 2.44 ± 0.33% ID/g), 44% (3.87 ± 0.30 vs 2.17 ± 0.13% ID/g) and 24% (10.69 ± 0.51 vs 8.13 ± 0.21% ID/g), respectively. No significant blocking changes were observed with [^{99m}Tc]Tc-EUKD-EDDA due to lower renal uptake.

The PK properties of [^{99m}Tc]Tc-EUKD-EDDA in blood within 30 min are shown in Figure 4c and Table S6. The main PK parameters of Lambda_z (λ), MRTlast and AUC_{0-t} were 0.019 min^{-1}, 1.76 and 290 min*%ID/g, respectively, and the theoretically predicted values of MRTINF_obs and $AUC_{0-\infty}$ were 13.08 and 337 min*%ID/g, respectively.

The biodistribution of [^{99m}Tc]Tc-EUKD-EDDA in the 22Rv1 mouse model was shown in Figure 4d and Table S7. The kidney was also the organ with the highest uptake (37.01 ± 2.09% ID/g, 2 h), followed by the tumor (4.58 ± 0.30% ID/g, 2 h). The uptake in blood, muscle, and bone was also less

https://doi.org/10.1021/acs.jmedchem.4c02656
J. Med. Chem. 2024, 67, 21617−21628

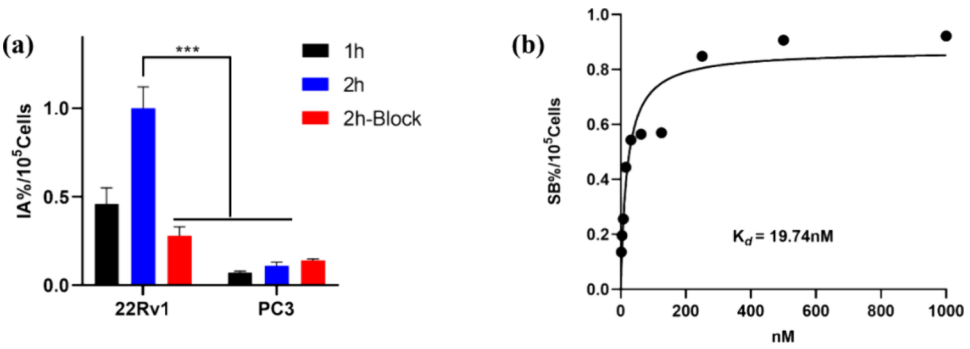

Figure 5. (a) Uptake of [^{99m}Tc]Tc-EUKD-EDDA in 22Rv1 (PSMA+) and PC3 (PSMA-) cells at 1 h, 2 and 2 h block. (b) Saturation binding experiments of [^{99m}Tc]Tc-EUKD-EDDA in 22Rv1 cells. *P < 0.05, **P < 0.01, ***P < 0.001.

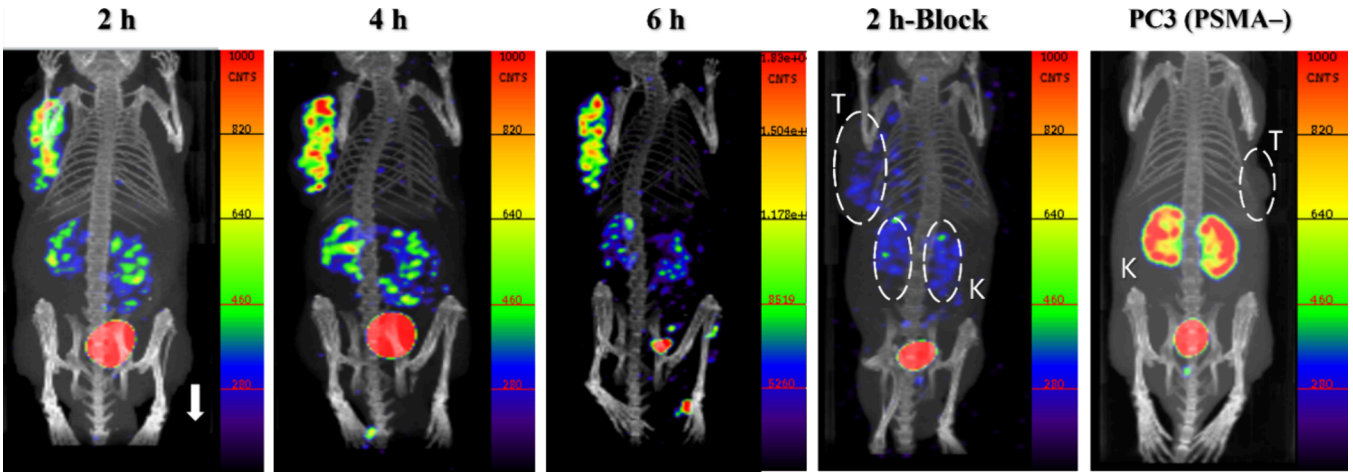

Figure 6. Micro SPECT/CT images of [^{99m}Tc]Tc-EUKD-EDDA in 22Rv1 or PC3 tumor-bearing male BALB/c nude mice at 2, 4, and 6 h after injection (T = tumor, K = kidney).

than 1% ID/g. In the presence of the blocking agent 2-PMPA, the uptake of the tracer in the tumor and kidney was effectively blocked, with BR of 73% (4.58 ± 0.30 vs 1.22 ± 0.09% ID/g) and 83% (37.01 ± 2.09 vs 6.23 ± 0.86% ID/g), respectively (Figure 4e). Over time, the tracer was continuously cleared from nontarget organs, and its uptake in the blood and muscles continued to decrease, particularly in the kidney (37.01 ± 2.09 vs 26.66 ± 3.83% ID/g, 2 h vs 4 h). Although tumor uptake also decreased over time (4.58 ± 0.30 vs 2.92 ± 0.29% ID/g, 2 h vs 4 h), the tumor-to-blood ratio (T/B) improved (4.66 vs 5.53, 2 h vs 4 h). Compared to the clearance rate of muscles, the clearance of tumors was significantly faster, resulting in a little decrease in tumor-to-muscle ratio (T/M) compared to 2 h, but still with higher contrast (10.03 vs 9.37, 2 h vs 4 h) (Figure 4f).

Cellular Uptake Studies. As shown in Figure 5a, the uptake of [^{99m}Tc]Tc-EUKD-EDDA in 22Rv1 cells (PSMA+) was significantly better than that in PC3 cells (PSMA-), regardless of whether it lasted 1 or 2 h, and a time-dependent uptake pattern appeared. In the presence of 2-PMPA, the uptake BR of the tracer in 22Rv1 cells was 72% after 2 h, whereas no difference in uptake was observed in PC3 cells. Moreover, as shown in Figure 5b, the nanomolar affinity (K_d = 19.74 nM) of the PSMA protein was measured via saturation competition experiments in 22Rv1 cells.

Micro-SPECT/CT Imaging Studies. SPECT/CT imaging of [^{99m}Tc]Tc-EUKD-EDDA in 22Rv1 and PC3 tumor-bearing mice is shown in Figures 6 and S2. [^{99m}Tc]Tc-EUKD-EDDA showed the best imaging properties: the tumor was clearly localized 2−6 h after injection and it was quickly eliminated via the kidney. [^{99m}Tc]Tc-EUKD-PG-EDDA and [^{99m}Tc]Tc-EUKD-PEG-EDDA also clearly imaged the tumor, but their uptake in the kidney was significantly greater than that of [^{99m}Tc]Tc-EUKD-EDDA (Figure S2a and **S2b**). Unfortunately, [^{99m}Tc]Tc-EUKT-EDDA did not show effective uptake in the tumor and showed high retention in the kidney (Figure S2c). Preinjection of 2-PMPA (500 μg) effectively blocked the accumulation of [^{99m}Tc]Tc-EUKD-EDDA in the tumor and kidney. Moreover, in the PC3 tumor-bearing mouse model, no uptake was observed in the tumor (PSMA-), but there was high retention in the kidney (PSMA+).

Molecular Dynamics and Docking Studies. Molecular docking (MD) and dynamics simulations (DS) theoretically confirmed the affinity of the tracer for the PSMA protein (PDB: 4LQG). As shown in Figures 7 and S3, Tc-EUKD-EDDA, Tc-EUKD-PG-EDDA and Tc-EUKD-PEG-EDDA formed stable complexes with proteins in the 50 ns kinetic simulation. Extensive hydrogen bonds and hydrophobic interactions formed with amino acid residues in the active pocket (Figures 7a and S3). However, Tc-EUKT-EDDA could not form an efficient complex with the PSMA protein. The root-mean-square deviation (RMSD) of the protein backbone and protein complex (Figures 7b and 7**c**) shows the stability of the tracer over the 50 ns simulation system and the reliability of the simulation result analysis. The root-mean-square fluctuation (RMSF) analysis of local flexibility (Figure 7d)

https://doi.org/10.1021/acs.jmedchem.4c02656
J. Med. Chem. 2024, 67, 21617−21628

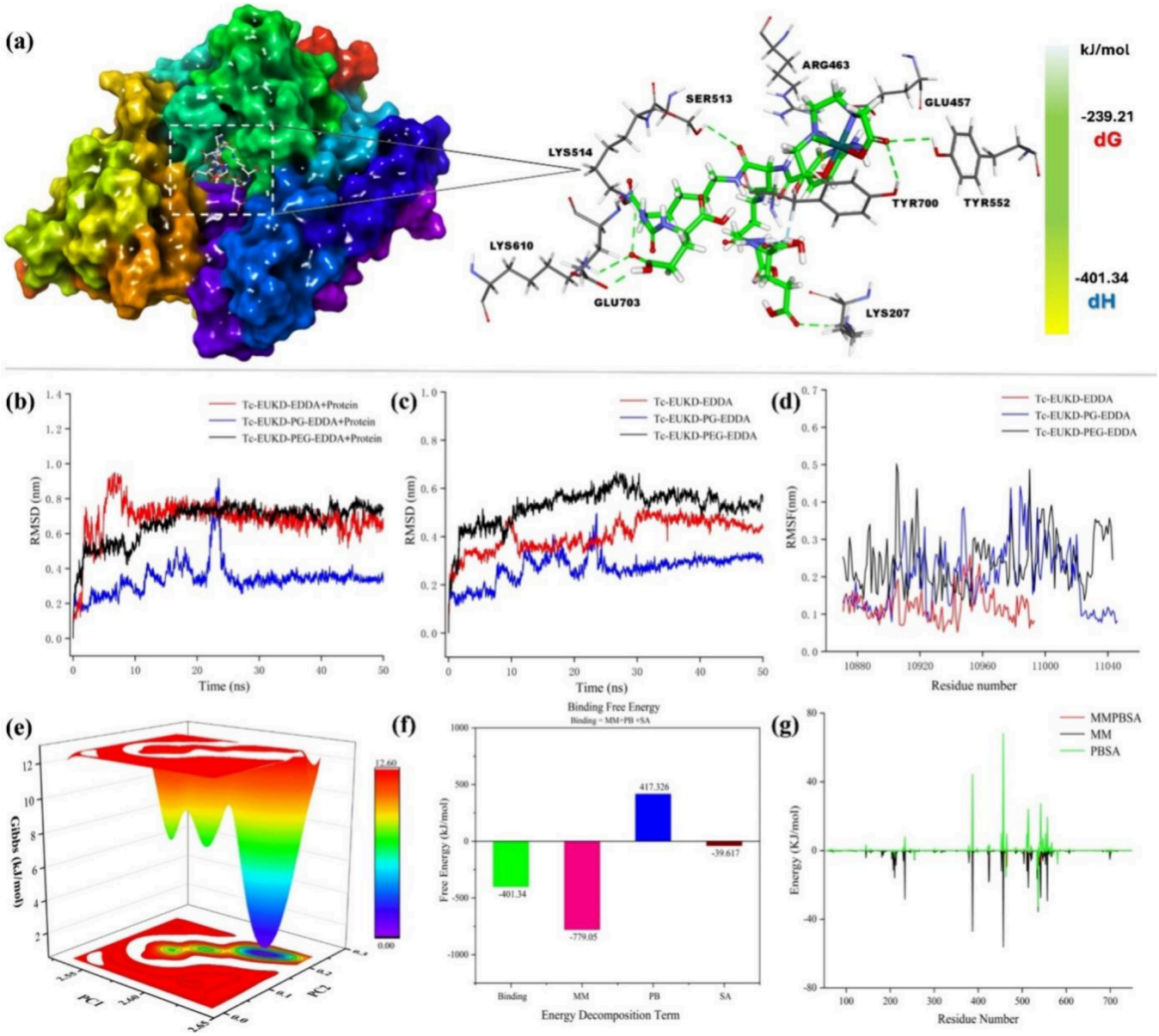

Figure 7. Molecular dynamics of radiotracers. (a) Interactions of Tc-EUKD-EDDA within protein cavities; (b) RMSD of the ligand−protein; (c) RMSD of the ligands; (d) RMSF of the ligands; (e) Gibbs energy landscape of Tc-EUKD-EDDA; (f) MMPBSA energy decomposition of Tc-EUKD-EDDA; (g) Contribution of protein residues to the MMPBSA energy of Tc-EUKD-EDDA.

revealed that the molecular structure of the tracer fluctuated significantly, which is further evidence of the tight binding of the ligand to the active cavity of the protein. Tc-EUKD-EDDA shows that there is only one lowest energy well in the entire simulation system (Figure 7e). The Molecular Mechanics Poisson−Boltzmann surface area (MMPBSA) energy calculation revealed that the total energy of the system is dG = −239.21 kJ/mol, of which the binding free energy is dH = −401.34 kJ/mol (including molecular mechanics energy (MM) = −779.05 kJ/mol, polarized solvation energy (PB) = 417.326 kJ/mol and nonpolar solvation energy (SA) = −39.617 kJ/mol). ARG463, GLU457, SER513 and LYS514, which form hydrogen bonds with Tc-EUKD-EDDA, are the main residues contributing energy (Figures 7f and 7g). The MMPBSA of Tc-EUKD-PG-EDDA and Tc-EUKD-PEG-EDDA were −193.016 kJ/mol and −136.72 kJ/mol, respectively (Table S8).

DISCUSSION

In this study, we designed and prepared 12 stable ^{99m}Tc-labeled PSMA polymer tracers by adjusting the number of EuKs, the type of linker between the targeting group and the chelators, and the composition of the coligand. This study will provides new insights into increasing the absolute tumor uptake of the tracer and reducing renal uptake. The ^{99m}Tc labeling method is simple, the radionuclide source is convenient, and the 12 stable PSMA polymer tracers can be used directly without purification (RCP > 90%), which is easy to promote and clinically apply.

All of the radiotracers showed good stability *in vitro*, and no significant degradation was observed in saline or fresh whole blood of mice within 4 h. All of the radiotracers were hydrophilic (Log P = −0.04 to −2.72), and [^{99m}Tc]Tc-EUKD-EDDA was the most hydrophilic. Coligands are an effective way to regulate the lipid−water distribution of radiotracers.

https://doi.org/10.1021/acs.jmedchem.4c02656
J. Med. Chem. 2024, 67, 21617−21628

EDDA and TPPTS improved the hydrophilicity of the tracer significantly better than TPPMS coligands did. Interestingly, among the two radioligands (EUKD and EUKT) without a linker introduced between the targeting group and the chelator, the coligand EDDA was more effective than TPPTS in improving the water solubility of the radiotracer. However, the opposite results were shown for the two radioligands EUKD-PG and EUKD-PEG (PG and PEG serve as linkers between the targeting group and the chelator). When comparing the relationship between the radiotracer Log *P* and the structure, one can clearly see that there is no obvious correlation between the two. It can be concluded that the regulation of lipid−water distribution is not only the result of the interaction of multiple functional groups but must also take into account the entire molecular structure. These results provide valuable insights into the design of HYNIC as a radiotracer for ^{99m}Tc-labeled chelators.

The preliminary PK properties of all of the radiotracers were studied in normal Kunming mice. A comparison of the effects of different coligands on the biodistribution of radiotracers revealed that the four radioligands presented the same trend. The elimination of the coligand EDDA in nontarget organs is significantly better than that of TPPTS and TPPMS, especially in metabolic organs such as the liver, spleen, lung, and kidney. The kidney is an organ with high PSMA expression and is also a dose-limiting organ for PSMA tracers.[11,21] The uptake level of radiotracers in the kidney has become an important reference indicator for our preliminary assessment of tracer performance. Among the four EDDA-labeled radiotracers, [^{99m}Tc]Tc-EUKD-EDDA showed the lowest renal uptake (1.58 ± 0.06% ID/g), followed by [^{99m}Tc]Tc-EUKD-PEG-EDDA (3.87 ± 0.30% ID/g) and [^{99m}Tc]Tc-EUKD-PG-EDDA (10.00 ± 0.50% ID/g), and [^{99m}Tc]Tc-EUKT-EDDA had the highest renal uptake (10.69 ± 0.51% ID/g). In addition to [^{99m}Tc]Tc-EUKD-EDDA, the three tracers could be effectively blocked by the PSMA blocker 2-PMPA, with renal BR of 76%, 44%, and 24%, respectively, indicating that they effectively target PSMA. [^{99m}Tc]Tc-EUKD-EDDA has an excellent renal clearance rate, maintaining renal uptake at a low level (probably basal uptake), so no significant renal blocking effect was observed. Moreover, all radiotracers can be quickly cleared (<1% ID/g, 2 h) from blood, muscle and bone, which has great potential for improving the TBRs of tracers.

[^{99m}Tc]Tc-EUKD-EDDA showed the best drug distribution and metabolism, and its PK properties in blood were examined from 0 to 30 min. The main PK parameters of tail vein injection Lambda_z (λ), MRTlast and AUC_{0-t} were 0.019 min^{-1}, 1.76 and 290 min*%ID/g, respectively, and the theoretically predicted values MRTINF_obs and $AUC_{0-\infty}$ were 13.08 and 337 min*%ID/g. The shorter residence time in the blood and the faster clearance rate provide powerful conditions for the rapid clearance of the tracer from the blood and its rapid distribution to other organs.

The biodistribution of [^{99m}Tc]Tc-EUKD-EDDA was studied in a 22Rv1 mouse model. At 2 h after injection, which is consistent with the observations in Kunming mice, the kidney was the organ with the highest dose (37.01 ± 2.09% ID/g), followed by the tumor (4.58 ± 0.30% ID/g). Compared with our previous studies on [^{99m}Tc]Tc-T-M2 and [^{99m}Tc]Tc-EUKPG-EDDA (single pharmacophore PSMA tracer, Figure S4),[37,38] the absolute uptake of [^{99m}Tc]Tc-EUKD-EDDA in tumors was significantly greater (4.58 ± 0.30 vs 2.15 ± 0.49 vs 1.07 ± 0.12% ID/g, 2 h). Compared with [^{99m}Tc]Tc-T-M2, renal uptake was significantly lower (37.01 ± 2.09 vs 72.66 ± 4.40% ID/g, 2 h). The main objective of this study was to increase absolute tumor uptake and TBRs by increasing the number of pharmacophores. Biodistribution in 22Rv1 tumor-bearing mice confirmed that this is a reasonable design strategy. At the same time, clearance in nontarget organs was faster, and uptake in blood, bone and muscle was less than 1% ID/g, resulting in higher TBRs. The T/B and T/M ratios were 4.66 and 10.03, respectively. Under the condition of preinjection of 2-PMPA (30 min in advance), the uptake of [^{99m}Tc]Tc-EUKD-EDDA into the kidney and tumor was significantly inhibited for 2 h after injection, with the BR of the kidney being 83% (37.01 ± 2.09 vs 6.23 ± 0.86% ID/g) and the BR of the tumor being 73% (4.58 ± 0.30 vs 1.22 ± 0.09% ID/g). The blocking experiment also demonstrated the high specificity of the tracer for PSMA. To further investigate the drug distribution and metabolic performance of the tracer over time, the biodistribution of [^{99m}Tc]Tc-EUKD-EDDA was examined in a 22Rv1 mouse model 4 h after injection under the same conditions. Compared with those at 2 h, all organs tended toward decreased uptake, and the kidney was still the organ with the highest uptake (26.66 ± 3.83% ID/g). Encouragingly, compared with that at 2 h, the retention rate of the tracer in the tumor reached 65% (4.58 ± 0.30 vs 2.92 ± 0.29% ID/g), which is also when the T/B ratio is considered to have increased to 5.53 and the T/M ratio is still as high as 9.37. The higher TBRs and good tumor retention effect give this tracer a clear advantage in time-lapse imaging.

The differential uptake of [^{99m}Tc]Tc-EUKD-EDDA in 22Rv1 (PSMA+) and PC3 (PSMA-) cells also showed high affinity for PSMA. The uptake of [^{99m}Tc]Tc-EUKD-EDDA in 22Rv1 cells was significantly greater than that in PC3 cells regardless of whether it lasted 1 or 2 h, and a time-dependent uptake pattern appeared. In the presence of 2-PMPA, the uptake BR of the tracer in 22Rv1 cells was 72% after 2 h, whereas no difference in uptake was observed in PC3 cells. The differential uptake and effective blocking of [^{99m}Tc]Tc-EUKD-EDDA in 22Rv1 and PC3 cells demonstrated that it targets the PSMA protein. Moreover, the nanomolar affinity (K_d = 19.74 nM) for the PSMA protein was measured via saturation competition experiments in 22Rv1 cells, which further demonstrated the high affinity of the tracer for the PSMA protein. The affinity of Tc-EUKD-EDDA for the PSMA protein was theoretically verified through MD and DS. Further analysis of the energy of the Tc-EUKD-EDDA protein complex revealed that there is only one lowest energy well in the entire simulation system, suggesting that Tc-EUKD-EDDA and the protein have only one lowest stable conformation. The MMPBSA energy calculation showed that the total energy of the system is dG = −239.21 kJ/mol, of which the binding free energy is dH = −401.34 kJ/mol (including MM = −779.05 kJ/mol, PB = 417.326 kJ/mol and SA = −39.617 kJ/mol), ARG463, GLU457, SER513 and LYS514, which form hydrogen bonds with Tc-EUKD-EDDA, are the main residues contributing energy.

[^{99m}Tc]Tc-EUKD-EDDA showed the best SPECT/CT imaging properties. The tumor was clearly localized for 2 h after injection and it was quickly eliminated via the kidney. As seen in the biodistribution, the higher TBRs enable the acquisition of high-contrast SPECT/CT images. [^{99m}Tc]Tc-EUKD-PG-EDDA and [^{99m}Tc]Tc-EUKD-PEG-EDDA also clearly imaged the tumor, but the uptake in the kidney was significantly greater than that of [^{99m}Tc]Tc-EUKD-EDDA,

https://doi.org/10.1021/acs.jmedchem.4c02656
J. Med. Chem. 2024, 67, 21617−21628

particularly [^{99m}Tc]Tc-EUKD-PEG-EDDA. Unfortunately, [^{99m}Tc]Tc-EUKT-EDDA did not show effective uptake in the tumor and showed high retention in the kidney. The results of MD and DS may provide a reasonable explanation for this phenomenon. Tc-EUKD-EDDA, Tc-EUKD-PG-EDDA and Tc-EUKD-PEG-EDDA can form stable complexes with proteins in the 50 ns kinetic simulation (MMPBSA: −239.21 vs −193.016 vs −136.72 kJ/mol). Extensive hydrogen bonds and hydrophobic interactions formed with amino acid residues in the active pocket. However, Tc-EUKT-EDDA could not form an efficient complex with the PSMA protein; this is consistent with the tracer imaging performance achieved by SPECT/CT. The mismatch between Tc-EUKT-EDDA and the active site of PSMA could be the main factor affecting the performance of this tracer, indicating that the molecular structure of Tc-EUKT-EDDA still needs to be further optimized. Recent studies have shown that time-lapse imaging of PSMA tracers has a positive impact compared with early imaging in detecting missed lesions, increasing image contrast, and accurately staging tumors.[39−41] Owing to its good tumor retention effect, [^{99m}Tc]Tc-EUKD-EDDA clearly localized to the tumor even after 4 and 6 h. Over time, the contrast of the SPECT/CT images obtained increased. This tracer has great application prospects in time-lapse imaging of PCa. Pre-injection of 2-PMPA (500 μg) effectively blocked the accumulation of [^{99m}Tc]Tc-EUKD-EDDA in the tumor and kidney. Moreover, in the PC3 tumor-bearing mouse model, no uptake was observed in the tumor (PSMA-), but high retention in the kidney (PSMA+) was detected. The differential uptake and effective blocking of [^{99m}Tc]Tc-EUKD-EDDA in 22Rv1 and PC3 tumor-bearing mice further confirmed its high affinity for the PSMA target. Therefore, both standard scan and time-lapse imaging, [^{99m}Tc]Tc-EUKD-EDDA has shown great potential for clinical application.

CONCLUSIONS

In this study, we designed and synthesized four radioligands targeting PSMA, including three dimers (EUKD, EUKD-PG, and EUKD-PEG) and one tetramer (EUKT). By coordinating ^{99m}Tc with various coligands, 12 stable radiotracers were prepared. All of the tracers had good stability, and preliminary PK studies were performed. [^{99m}Tc]Tc-EUKD-EDDA showed the best PK properties and could bind stably in the active cavity of the PSMA protein, showed nanomolar affinity (K_d = 19.74 nM), and exhibited significant tumor uptake in cell and SPECT imaging. [^{99m}Tc]Tc-EUKD-EDDA effectively increased the absolute uptake in tumors and resulted in good tumor retention. Its rapid clearance in nontarget organs resulted in high TBRs. More importantly, high-contrast SPECT/CT images can be obtained within 2−6 h after injection, providing the obvious advantage of time-lapse imaging; this is meaningful for improving the diagnostic accuracy of PCa in the clinic, particularly in detecting recurrences and distinguishing tumors from nonneoplastic lesions, helping to more accurately stage and guide treatment decisions. In conclusion, [^{99m}Tc]Tc-EUKD-EDDA is a promising candidate for PSMA-targeted tumor imaging agents.

EXPERIMENTAL SECTION

General. Unless otherwise stated, all reactions were carried out in flame-dried glass vessels with magnetic stirring in a nitrogen atmosphere. All reagents were purchased from Tong Guang Fine Chemicals Company (Beijing, China), Aladdin, Innochem, and JandK. Nuclear magnetic resonance (NMR) spectra of ^{1}H were obtained via a 400 or 600 MHz JNM-ECS spectrometer (JEOL, Tokyo, Japan). The NMR chemical shifts were compared to those of the internal standard, TMS, or to residual solvent peaks. Each coupling constant J was given in Hertz (Hz). Mass spectra (MS) were acquired using ESI ionization on a Thermo Scientific LCQ mass spectrometer (Thermo, USA). A Kromasil C18 column (250 × 4.6 mm, 5 μm) on a Shimadzu 20A (Shimadzu, Kyoto, Japan) was used for the radioactive high-performance liquid chromatography (R-HPLC) analyses. Saline was used to elute [^{99m}Tc]$NaTcO_4$ with a ^{99m}Mo/^{99m}Tc generator purchased from Zhibo Biomedical Tech (Beijing, China). A Wizard 2480 γ-counter (PerkinElmer, Singapore) and an HRS-1000 technetium analyzer (Huaruison, Beijing, China) were used to measure radioactivity. The Typical Culture Collection of the Chinese Academy of Sciences (Beijing, China) provided the 22Rv1 and PC3 cell lines. *In vivo* imaging studies were performed using a micro-SPECT/CT device (Trifoil, CA).

Radiolabeling. *[^{99m}Tc]Tc-EUKD-TPPTS.* Tricine (1 mg) and TPPTS (2 mg) were dissolved in 0.5 mL of phosphate-buffered saline (PBS). To this mixture, succinate buffer adjusted to a pH of 6.0 was added (0.3 mL), followed by EUKD (20 μg) and 0.5 mL of freshly eluted [^{99m}Tc]$NaTcO_4$ (37−370 MBq) in sequence, and the mixture was then subjected to a reaction at 100 °C for 30 min to yield the radiotracer [^{99m}Tc]Tc-EUKD-TPPTS.

[^{99m}Tc]Tc-EUKD-TPPMS. Tricine (1 mg) and TPPMS (2 mg) were dissolved in 0.5 mL of PBS. To this mixture, succinate buffer adjusted to a pH of 6.0 was added (0.3 mL), followed by EUKD (20 μg) and 0.5 mL of freshly eluted [^{99m}Tc]$NaTcO_4$ (37−370 MBq) in sequence, and the mixture was then subjected to a reaction at 100 °C for 30 min to yield the radiotracer [^{99m}Tc]Tc-EUKD-TPPMS.

[^{99m}Tc]Tc-EUKD-EDDA. Tricine (20 mg) and EDDA (10 mg) were dissolved in 0.5 mL of PBS. To this solution, succinate buffer adjusted to a pH of 7.0 was added (0.2 mL), the solution pH was adjusted to 7.0−8.0 with NaOH (1 mol/L), followed by EUKD (20 μg), $SnCl_2 \cdot 2H_2O$ (100 μg) and 0.5 mL of freshly eluted [^{99m}Tc]$NaTcO_4$ (37−370 MBq) in sequence, and the mixture was then subjected to a reaction at 100 °C for 20 min to yield the radiotracer [^{99m}Tc]Tc-EUKD-EDDA.

The labeling methods of [^{99m}Tc]Tc-EUKD-PG-TPPTS, [^{99m}Tc]-Tc-EUKD-PEG-TPPTS and [^{99m}Tc]Tc-EUKT-TPPTS were the same as that of [^{99m}Tc]Tc-EUKD-TPPTS. The labeling methods of [^{99m}Tc]Tc-EUKD-PG-TPPMS, [^{99m}Tc]Tc-EUKD-PEG-TPPMS and [^{99m}Tc]Tc-EUKT-TPPMS were the same as that of [^{99m}Tc]Tc-EUKD-TPPMS. The labeling methods of [^{99m}Tc]Tc-EUKD-PG-EDDA, [^{99m}Tc]Tc-EUKD-PEG-EDDA and [^{99m}Tc]Tc-EUKT-EDDA were the same as that of [^{99m}Tc]Tc-EUKD-EDDA.

All ^{99m}Tc-labeled complexes do not require purification, with a RCP of >90%.

R-HPLC Analysis and Stability Assay. R-HPLC was used to measure the RCP and stability of the ^{99m}Tc-labeled radiotracers. R-HPLC analysis was performed on a Shimadzu 20A instrument equipped with a Kromasil C18 column (250 × 4.6 mm, 5 μm). The injection volume was 10 μL. The flow rate was 1.0 mL/min. Phase B was acetonitrile, and phase A was water with 0.1% TFA. The R-HPLC program was as follows: 10% phase B (stationary from 0 to 2 min), 10%−90% phase B (linear increase from 2 to 5 min), 90% phase B (stationary time 5 to 20 min), and 90%−10% phase B (linear decrease from 20 to 30 min).

The *in vitro* stability of mouse whole blood and saline was assessed. After storing the radiolabeled solution at 37 °C for 4 h, R-HPLC was used to determine the RCP. The radiotracers were incubated with fresh mouse blood in equal parts (v/v) for 4 h at 37 °C to measure whole blood stability. A solvent mixture of acetonitrile and ethanol at a ratio of 1:2 was then added to the incubated mixture to extract the plasma proteins. The mixture was centrifuged at 4 °C and 12,000 rpm for 5 min. The supernatant was then filtered with a 0.22 μm filter membrane, and R-HPLC analysis was performed to determine the RCP.

Octanol/Water Partition Coefficient (Log *P*). The shake flask method was used to test the Log *P* values of the radiotracers. PBS

https://doi.org/10.1021/acs.jmedchem.4c02656
J. Med. Chem. 2024, 67, 21617−21628

(0.025% mol/L, pH 7.4) was used overnight to presaturate the *n*-octanol used in the experiment. In summary, 900 μL of PBS, 1 mL of *n*-octanol, and 100 μL of radiotracer were added to a centrifuge tube, and the mixture was shaken vigorously for 5 min. To achieve phase separation, the mixture was then centrifuged at 10,000 rpm for 15 min. Then, 500 μL samples of PBS and *n*-octanol were collected and analyzed via a γ-counter. To determine the distribution coefficient, the radioactivity counts in the two phases were compared. Log *P* = log (cpm in *n*-octanol/cpm in PBS) was used to calculate the results from three parallel experiments. Log *P* values were expressed as the means ± SDs.

Cell Culture and Tumor Models. The 22Rv1 (PSMA+) and PC3 (PSMA-) cancer cell lines were cultured in RPMI 1640 medium supplemented with 10% (v/v) heat-inactivated fetal bovine serum (FBS) and 1% (v/v) penicillin−streptomycin at 37 °C in a cell culture incubator with 5% CO_2.

All of the mice were purchased from the Shibeifu Experimental Animal Company (Beijing, China). All animals were raised in a pathogen-free 26 °C environment with ample space for movement, socialization, and natural behaviors. They had continuous access to clean water and a balanced feed. All of the animal protocols were approved and supervised by the Institutional Animal Care and Use Committee of Beijing Normal University. Male Kunming mice (4−5 weeks old) were used in the preliminary PK experiments. 22Rv1 or PC3 cells (approximately 1×10^7) suspended in PBS (100 μL) were injected subcutaneously into the flanks of male BALB/c nude mice (4−5 weeks old), and biodistribution and SPECT imaging were performed in the 22Rv1 and PC3 mouse models 3 weeks later (the tumor diameter was approximately 5−12 mm).

Biodistribution Studies in Mice. In the preliminary PK study of all of the radiotracers, Kunming mice (n = 5) were used for evaluation. Each mouse received an injection of ^{99m}Tc-labeled tracer (1.85 ± 0.05 MBq, 100 μL) through the tail vein, and the mice were sacrificed 2 h after injection. Blood as well as major organs such as the heart, liver, spleen, lung, kidney, muscle, bone, stomach, brain, large intestine, and small intestine were collected, weighed, and counted with a γ-counter. Preinjected mice in the blocking study received the PSMA-selective inhibitor 2-PMPA (500 μg, 100 μL) 30 min prior. They then received an intravenous injection of the ^{99m}Tc-labeled tracer (1.85 ± 0.05 MBq/100 μL) and were sacrificed 2 h after the injection. The biodistribution study in the 22Rv1 mouse model (n = 3) was the same as above, and the data obtained are expressed as the percentage of intake of the injected dose per gram of organ or tissue (% ID/g), and the values were expressed as the means ± SDs.

Similar to the biodistribution in Kunming mice, blood samples were collected at 0 min, 5 min, 15 and 30 min after injection, and their radioactivity was detected via a γ-counter. Blood PK parameters were determined by fitting the noncompartmental model in Phoenix software based on the trend of radioactivity in blood over time.

Cellular Uptake and Saturation Binding Assay *In Vitro*. 22Rv1 and PC3 cells were seeded in 24-well plates (1×10^5 cells per well) and incubated overnight. Each well was filled with 0.5 mL of fresh culture medium containing [^{99m}Tc]Tc-EUKD-EDDA (0.37 MBq). After 1 or 2 h, the culture medium was removed, and the cells were washed twice with cold PBS before being lysed with 1 M NaOH. A γ-counter was used to quantify the radioactivity. In the blocking experiment, the experimental group's workflow was followed after the PSMA inhibitor 2-PMPA (1 μM) was used for intervention 30 min prior. The data are presented as the means ± SDs, and the results are expressed as the percentage of injected activity (IA %)/10^5 cells relative to the 22Rv1 control group.

The literature instructions for performing saturation binding tests were followed.[37] 22Rv1 cells were treated with different concentrations of [^{99m}Tc]Tc-EUKGP-EDDA (1.56−1000 nM) in 96-well plates. The inhibition group (500 nM per well) was subjected to intervention 30 min in advance. After incubation for 1 h, the medium was removed, the cells were subjected to two cold PBS washes and lysed with 1 M NaOH, and the radioactivity was assessed with a γ-counter. The specific binding percentage (SB %)/10^5 cells was used to present the results. GraphPad Prism 8.2 was used to calculate the dissociation constant (K_d) based on the acquired data to determine the PSMA affinity.

Small Animal Micro-SPECT/CT Imaging. [^{99m}Tc]Tc-EUKD-EDDA, [^{99m}Tc]Tc-EUKD-PG-EDDA, [^{99m}Tc]Tc-EUKD-PEG-EDDA and [^{99m}Tc]Tc-EUKT-EDDA (37 MBq, 100 μL) were injected intravenously into 22Rv1 or PC3 model mice (n = 3). The mice were initially administered 3% (v/v) isoflurane anesthesia, and static scanning with 1.5% isoflurane in air at 500 mL/min was used to perform SPECT/CT at 2 and 4 h after injection to obtain images. Blockade studies were performed in mice bearing 22Rv1 tumors by preinjecting 2-PMPA (500 μg) via the tail vein 30 min in advance and then injecting 100 μL of the above radiotracers (37 MBq). The mice in the anesthesia blocking group were maintained under the same conditions, and images were taken 2 h after injection.

Molecular Docking and Dynamics Assay. The Auto Dock 4.2 workspace was used for molecular docking. The docking receptor used in this experiment was the protein crystal structure (PDB: 4LQG) obtained from the protein data bank (PDB). The target molecule was used in the Gaussian 09 workspace for 3D structural optimization docking simulations with the Amber 99 force field. The cocrystallized ligand served as the docking center, and there were no limitations in defining the binding sites for subsequent docking studies using the default settings. The preliminary docking results were subjected to molecular dynamics in Gromacs 2020, using the GAFF atomic model for small-molecule optimization. Amber 99 force for protein structure optimization, SPC for the water model, and NVT and NPT pre-equilibration for 2 ns were used and the dynamic simulation time was 50 ns. The RMSD and RMSF of the molecular dynamics results were examined. The energy results of the MMPBSA calculation were decomposed after the last 10 ns was completed. The final conformation displayed and examined in PyMOL was the final image of the simulation results.

■ ASSOCIATED CONTENT

Supporting Information

The Supporting Information is available free of charge at https://pubs.acs.org/doi/10.1021/acs.jmedchem.4c02656.

Synthesis of the radioligand, radiotracer stability and Log *P*, biodistribution, micro-SPECT/CT imaging, molecular dynamics, and ^{1}H NMR and MS spectra (PDF)

Molecular formula strings (CSV)

■ AUTHOR INFORMATION

Corresponding Author

Junbo Zhang − *Key Laboratory of Radiopharmaceuticals of the Ministry of Education, College of Chemistry, NMPA Key Laboratory for Research and Evaluation of Radiopharmaceuticals (National Medical Products Administration), Beijing Normal University, Beijing 100875, P. R. China*; orcid.org/0000-0003-3549-6483; Email: zhjunbo@bnu.edu.cn

Authors

Zuojie Li − *Key Laboratory of Radiopharmaceuticals of the Ministry of Education, College of Chemistry, NMPA Key Laboratory for Research and Evaluation of Radiopharmaceuticals (National Medical Products Administration), Beijing Normal University, Beijing 100875, P. R. China*

Xiaojiang Duan − *Department of Nuclear Medicine, Peking University First Hospital, Beijing 100034, P. R. China*

Peiwen Han − *Key Laboratory of Radiopharmaceuticals of the Ministry of Education, College of Chemistry, NMPA Key Laboratory for Research and Evaluation of Radiopharmaceuticals (National Medical Products*

Administration), Beijing Normal University, Beijing 100875, P. R. China

Guangxing Yin − *Key Laboratory of Radiopharmaceuticals of the Ministry of Education, College of Chemistry, NMPA Key Laboratory for Research and Evaluation of Radiopharmaceuticals (National Medical Products Administration), Beijing Normal University, Beijing 100875, P. R. China*

Yuhao Jiang − *Key Laboratory of Radiopharmaceuticals of the Ministry of Education, College of Chemistry, NMPA Key Laboratory for Research and Evaluation of Radiopharmaceuticals (National Medical Products Administration) and Key Laboratory of Beam Technology of the Ministry of Education, College of Physics and Astronomy, Beijing Normal University, Beijing 100875, P. R. China;* orcid.org/0009-0004-9436-7109

Qing Ruan − *Key Laboratory of Radiopharmaceuticals of the Ministry of Education, College of Chemistry, NMPA Key Laboratory for Research and Evaluation of Radiopharmaceuticals (National Medical Products Administration) and Key Laboratory of Beam Technology of the Ministry of Education, College of Physics and Astronomy, Beijing Normal University, Beijing 100875, P. R. China;* orcid.org/0000-0003-1586-1682

Complete contact information is available at: https://pubs.acs.org/10.1021/acs.jmedchem.4c02656

Notes

The authors declare no competing financial interest.

■ ACKNOWLEDGMENTS

This work was financially supported, in part, by the Beijing Natural Science Foundation (2232010), the National Natural Science Foundation of China (22076013, 22276015, 22476011), and the Beijing Nova Program (20230484470).

■ ABBREVIATIONS

BR, blocking rate; DS, dynamics simulations; EDDA, ethylenediaminediacetic acid; EuK, glu-urea-lysine; EuKs, EuK groups; FAP, fibroblast activation protein; tricine, *N*-[tris(hydroxymethyl)methyl]glycine; HATU, hexafluorophosphate azabenzotriazole tetramethyl uronium; HYNIC, hydrazinonicotinamide; IA, injected activity; MD, molecular docking; MM, molecular mechanics energy; MMPBSA, molecular mechanicspoisson-boltzmann surface area; MS, mass spectra; NMR, nuclear magnetic resonance; PB, polarized solvation energy; PBS, phosphate buffered saline; PCa, prostate cancer; PDB, Protein Data Bank; PEG, polyethylene glycol; PET, positron emission tomography; PG, $_{D}$Pro-Gly; PK, pharmacokinetic; PSA, prostate-specific antigen; PSMA, prostate-specific membrane antigen; RCP, radiochemical puritys; R-HPLC, radioactive high-performance liquid chromatography; RMSD, root-mean-square deviation; RMSF, root-mean-square fluctuation; SA, nonpolar solvation energy; SB, specific binding; SPECT, single photon emission computed tomography; TBRs, tumor-to-background ratios; TPPTS, triphenylphosphine trisulfonate; TPPMS, diphenylphosphine benzene-3-sulfonate

■ REFERENCES

(1) Sallam, M.; Nguyen, N.-T.; Sainsbury, F.; Kimizuka, N.; Muyldermans, S.; Benešová-Schäfer, M. PSMA-Targeted Radiotheranostics in Modern Nuclear Medicine: Then, Now, and What of the Future? *Theranostics* **2024**, *14* (8), 3043−3079.

(2) Uijen, M. J. M.; Derks, Y. H. W.; Merkx, R. I. J.; Schilham, M. G. M.; Roosen, J.; Privé, B. M.; van Lith, S. A. M.; van Herpen, C. M. L.; Gotthardt, M.; Heskamp, S.; et al. PSMA Radioligand Therapy for Solid Tumors Other than Prostate Cancer: Background, Opportunities, Challenges, and First Clinical Reports. *Eur. J. Nucl. Med. Mol. Imaging* **2021**, *48* (13), 4350−4368.

(3) O'Keefe, D. S.; Bacich, D. J.; Huang, S. S.; Heston, W. D. W. A Perspective on the Evolving Story of PSMA Biology, PSMA-Based Imaging, and Endoradiotherapeutic Strategies. *J. Nucl. Med.* **2018**, *59* (7), 1007−1013.

(4) Murphy, D. G.; Sathianathen, N.; Hofman, M. S.; Azad, A.; Lawrentschuk, N. Where to Next for Theranostics in Prostate Cancer? *Eur. Urol Oncol* **2019**, *2* (2), 163−165.

(5) Siegel, R. L.; Giaquinto, A. N.; Jemal, A. Cancer Statistics, 2024. *CA Cancer J. Clin* **2024**, *74* (1), 12−49.

(6) Cui, X. Y.; Liu, Y.; Wang, C.; Wen, Z.; Li, Y.; Tang, H.; Diwu, J.; Yang, Y.; Cui, M.; Liu, Z. China's Radiopharmaceuticals on Expressway: 2014−2021. *Radiol Acta* **2022**, *110* (6−9), 765−784.

(7) Mehra, R.; Kumar-Sinha, C.; Shankar, S.; Lonigro, R. J.; Jing, X.; Philips, N. E.; Siddiqui, J.; Han, B.; Cao, X.; Smith, D. C.; et al. Characterization of Bone Metastases from Rapid Autopsies of Prostate Cancer Patients. *Clin. Cancer Res.* **2011**, *17* (12), 3924−3932.

(8) Haberkorn, U.; Eder, M.; Kopka, K.; Babich, J. W.; Eisenhut, M. New Strategies in Prostate Cancer: Prostate-Specific Membrane Antigen (PSMA) Ligands for Diagnosis and Therapy. *Clin. Cancer Res.* **2016**, *22* (1), 9−15.

(9) Mottet, N.; van den Bergh, R. C. N.; Briers, E.; Van den Broeck, T.; Cumberbatch, M. G.; De Santis, M.; Fanti, S.; Fossati, N.; Gandaglia, G.; Gillessen, S.; et al. Eau-Eanm-Estro-Esur-Siog Guidelines on Prostate Cancer-2020 Update. Part 1: Screening, Diagnosis, and Local Treatment with Curative Intent. *Eur. Urol* **2021**, *79* (2), 243−262.

(10) Cornford, P.; van den Bergh, R. C. N.; Briers, E.; Van den Broeck, T.; Cumberbatch, M. G.; De Santis, M.; Fanti, S.; Fossati, N.; Gandaglia, G.; Gillessen, S.; et al. Eau-Eanm-Estro-Esur-Siog Guidelines on Prostate Cancer. Part II-2020 Update: Treatment of Relapsing and Metastatic Prostate Cancer. *Eur. Urol* **2021**, *79* (2), 263−282.

(11) Fanti, S.; Minozzi, S.; Antoch, G.; Banks, I.; Briganti, A.; Carrio, I.; Chiti, A.; Clarke, N.; Eiber, M.; De Bono, J.; et al. Consensus on Molecular Imaging and Theranostics in Prostate Cancer. *Lancet Oncol* **2018**, *19* (12), e696−e708.

(12) Toyohara, J.; Vugts, D.; Kiss, O. C.; Todde, S.; Li, X.-G.; Liu, Z.; Yang, Z.; Gillings, N.; Cazzola, E.; Szymanski, W.; et al. Highlight Selection of Radiochemistry and Radiopharmacy Developments by Editorial Board. *EJNMMI Radiopharmacy Chem.* **2024**, *9* (1), 42−62.

(13) Yang, W.; Kang, F.; Chen, Y.; Zhu, Z.; Wang, F.; Qin, C.; Du, J.; Lan, X.; Wang, J. Landscape of Nuclear Medicine in China and Its Progress on Theranostics. *J. Nucl. Med.* **2024**, *65* (Supplement 1), 29S−37S.

(14) van der Meulen, N. P.; Strobel, K.; Lima, T. V. M. New Radionuclides and Technological Advances in SPECT and PET Scanners. *Cancers (Basel)* **2021**, *13* (24), 6183−6198.

(15) Rong, J.; Haider, A.; Jeppesen, T. E.; Josephson, L.; Liang, S. H. Radiochemistry for Positron Emission Tomography. *Nat. Commun.* **2023**, *14* (1), 3257−3279.

(16) Aboagye, E. O.; Barwick, T. D.; Haberkorn, U. Radiotheranostics in Oncology: Making Precision Medicine Possible. *CA Cancer J. Clin* **2023**, *73* (3), 255−274.

(17) Lunger, L.; Chantadisai, M.; Karimzadeh, A.; Rauscher, I.; D'Alessandria, C.; Feuerecker, B.; Langbein, T.; Tauber, R.; Schiele, S.; Weber, W.; et al. Prognostic Role of ^{68}Ga-PSMA11 PET-Based Response in Patients with Prostate Cancer Undergoing Taxane-Based Chemotherapy. *J. Nucl. Med.* **2023**, *64* (6), 896−901.

(18) Yusufi, N.; Wurzer, A.; Herz, M.; D'Alessandria, C.; Feuerecker, B.; Weber, W.; Wester, H. J.; Nekolla, S.; Eiber, M. Comparative

Preclinical Biodistribution, Dosimetry, and Endoradiotherapy in Metastatic Castration-Resistant Prostate Cancer Using $^{19}F/^{177}Lu$-RhPSMA-7.3 and ^{177}Lu-PSMA I&T. *J. Nucl. Med.* **2021**, *62* (8), 1106−1111.
(19) Czernin, J.; Calais, J. ^{177}Lu-PSMA617 and the Vision Trial: One of the Greatest Success Stories in the History of Nuclear Medicine. *J. Nucl. Med.* **2021**, *62* (8), 1025−1026.
(20) Ferro-Flores, G.; Luna-Gutiérrez, M.; Ocampo-García, B.; Santos-Cuevas, C.; Azorín-Vega, E.; Jiménez-Mancilla, N.; Orocio-Rodríguez, E.; Davanzo, J.; García-Pérez, F. O. Clinical Translation of a PSMA Inhibitor for ^{99m}Tc-Based SPECT. *Nucl. Med. Biol.* **2017**, *48*, 36−44.
(21) Neels, O. C.; Kopka, K.; Liolios, C.; Afshar-Oromieh, A. Radiolabeled PSMA Inhibitors. *Cancers* **2021**, *13* (24), 6255−6278.
(22) Ehlerding, E. B.; Sun, L.; Lan, X.; Zeng, D.; Cai, W. Dual-Targeted Molecular Imaging of Cancer. *J. Nucl. Med.* **2018**, *59* (3), 390−395.
(23) Chen, H.; Niu, G.; Wu, H.; Chen, X. Clinical Application of Radiolabeled RGD Peptides for PET Imaging of Integrin $\alpha_v\beta_3$. *Theranostics* **2016**, *6* (1), 78−92.
(24) Zhang, H.; Rao, M.; Zhao, H.; Ren, J.; Hao, L.; Zhong, M.; Chen, Y.; Yang, X.; Feng, Y.; Yuan, G. Imageological/Structural Study Regarding the Improved Pharmacokinetics by ^{68}Ga-Labeled Pegylated PSMA Multimer in Prostate Cancer. *Pharmaceuticals* **2023**, *16* (4), 589−603.
(25) Chen, Y.; Zhang, X.; Ni, M.; Gao, X.; Wang, X.; Xie, Q.; Zhang, J.; Cui, M. Synthesis, Preclinical Evaluation, and First-in-Human PET Study of [^{68}Ga]-Labeled Biphenyl-Containing PSMA Tracers. *J. Med. Chem.* **2023**, *66* (18), 13332−13345.
(26) Schäfer, M.; Bauder-Wüst, U.; Leotta, K.; Zoller, F.; Mier, W.; Haberkorn, U.; Eisenhut, M.; Eder, M. A Dimerized Urea-Based Inhibitor of the Prostate-Specific Membrane Antigen for ^{68}Ga-PET Imaging of Prostate Cancer. *EJNMMI Res.* **2012**, *2* (1), 23−34.
(27) Zhu, Z.; Miao, W.; Li, Q.; Dai, H.; Ma, Q.; Wang, F.; Yang, A.; Jia, B.; Jing, X.; Liu, S.; et al. ^{99m}Tc-3PRGD$_2$ for Integrin Receptor Imaging of Lung Cancer: A Multicenter Study. *J. Nucl. Med.* **2012**, *53* (5), 716−722.
(28) Zhao, L.; Niu, B.; Fang, J.; Pang, Y.; Li, S.; Xie, C.; Sun, L.; Zhang, X.; Guo, Z.; Lin, Q.; et al. Synthesis, Preclinical Evaluation, and a Pilot Clinical PET Imaging Study of ^{68}Ga-Labeled FAPi Dimer. *J. Nucl. Med.* **2022**, *63* (6), 862−868.
(29) Pang, Y.; Zhao, L.; Fang, J.; Chen, J.; Meng, L.; Sun, L.; Wu, H.; Guo, Z.; Lin, Q.; Chen, H. Development of FAPi Tetramers to Improve Tumor Uptake and Efficacy of FAPi Radioligand Therapy. *J. Nucl. Med.* **2023**, *64* (9), 1449−1455.
(30) Mizuno, Y.; Kimura, K.; Onoe, S.; Shukuri, M.; Kuge, Y.; Akizawa, H. Influence of Linker Molecules in Hexavalent RGD Peptides on Their Multivalent Interactions with Integrin $\alpha_v\beta_3$. *J. Med. Chem.* **2021**, *64* (21), 16008−16019.
(31) Ruan, Q.; Wang, Q. N.; Jiang, Y. H.; Feng, J. H.; Yin, G. X.; Zhang, J. B. Synthesis and Evaluation of ^{99m}Tc-Labeled FAP Inhibitors with Different Linkers for Imaging of Fibroblast Activation Proteins in Tumors. *J. Med. Chem.* **2023**, *66* (7), 4952−4960.
(32) Ruan, Q.; Ding, D. J.; Diao, L. A.; Feng, J. H.; Yin, G. X.; Jiang, Y. H.; Wang, Q. N.; Han, P. W.; Jiang, J. Y.; Zhang, J. B. Synthesis and Preclinical Evaluation of Novel ^{99m}Tc-Labeled FAPi-46 Derivatives with Significant Tumor Uptake and Improved Tumor-to-Nontarget Ratios. *J. Med. Chem.* **2024**, *67* (4), 3190−3202.
(33) Ruan, Q.; Feng, J.; Jiang, Y.; Zhang, X.; Duan, X.; Wang, Q.; Yin, G.; Xiao, D.; Zhang, J. Preparation and Bioevaluation of ^{99m}Tc-Labeled FAP Inhibitors as Tumor Radiotracers to Target the Fibroblast Activation Protein. *Mol. Pharm.* **2022**, *19* (1), 160−171.
(34) Leopold, C. S.; Friend, D. R. *In Vivo* Pharmacokinetic Study for the Assessment of Poly(L-Aspartic Acid) as a Drug Carrier for Colon-Specific Drug Delivery. *J. Pharmacokinet. Biopharm.* **1995**, *23* (4), 397−406.
(35) Duatti, A. Review on ^{99m}Tc Radiopharmaceuticals with Emphasis on New Advancements. *Nucl. Med. Biol.* **2021**, *92*, 202−216.
(36) Shi, J.; Liu, S. Clinical Application of ^{99m}Tc-Labeled Peptides for Tumor Imaging: Current Status and Future Directions. *iRADIOLOGY* **2024**, *2* (1), 17−34.
(37) Li, Z.; Jiang, Y.; Ruan, Q.; Yin, G.; Han, P.; Duan, X.; Zhang, J. Synthesis and Evaluation of ^{99m}Tc-Labeled $_D$Pro-Gly-Containing Tracers Targeting PSMA. *Mol. Pharmaceutics* **2024**, *21* (10), 5305−5314.
(38) Xiao, D.; Han, P. W.; Jiang, Y. H.; Duan, X. J.; Ruan, Q.; Zhang, Z. B.; Chen, X. L.; Zhang, J. B. Preparation, Biological Evaluation, and First-in-Human Single-Photon Emission Computed Tomography (SPECT) Study of ^{99m}Tc-Labeled Prostate-Specific Membrane Antigen (PSMA)-Targeted Radiotracers Containing Triazole with Reduced Kidneys Accumulation. *ACS Pharmacol Transl Sci.* **2024**, *7* (5), 1335−1347.
(39) Unterrainer, L. M.; Ruchalski, K.; Allen-Auerbach, M. S.; Calais, J.; Benz, M. R. PSMA PET/CT Dual-Time-Point Imaging: Nice to Have or Need to Have? *J. Nucl. Med.* **2024**, *65* (5), 818−819.
(40) Morawitz, J.; Kirchner, J.; Hertelendy, J.; Loberg, C.; Schimmöller, L.; Dabir, M.; Häberle, L.; Mamlins, E.; Antke, C.; Arsov, C.; et al. Is There a Diagnostic Benefit of Late-Phase Abdomino-Pelvic PET/CT after Urination as Part of Whole-Body ^{68}Ga-PSMA-11 PET/CT for Restaging Patients with Biochemical Recurrence of Prostate Cancer after Radical Prostatectomy? *EJNMMI Res.* **2022**, *12* (1), 12−20.
(41) Bauckneht, M.; Miceli, A.; Signori, A.; Albano, D.; Capitanio, S.; Piva, R.; Laudicella, R.; Franchini, A.; D'Amico, F.; Riondato, M.; et al. Combined Forced Diuresis and Late Acquisition on [^{68}Ga]Ga-PSMA-11 PET/CT for Biochemical Recurrent Prostate Cancer: A Clinical Practice-Oriented Study. *Eur. Radiol* **2023**, *33* (5), 3343−3353.

https://doi.org/10.1021/acs.jmedchem.4c02656
J. Med. Chem. 2024, 67, 21617−21628